Catalysis Today 215 (2013) 260–266

Contents lists available at SciVerse ScienceDirect

Catalysis Today

journal homepage: www.elsevier.com/locate/cattod

Production of ethanol by gas phase hydrogenation of acetic acid over carbon nanotube-supported Pt–Sn nanoparticles

Subin Zhang, Xinping Duan, Linmin Ye, Haiqiang Lin, Zhaoxiong Xie*, Youzhu Yuan*

State Key Laboratory for Physical Chemistry of Solid Surfaces, National Engineering Laboratory for Green Chemical Productions of Alcohols-Ethers-Esters, College of Chemistry and Chemical Engineering, Xiamen University, Xiamen 361005, China

ARTICLE INFO

Article history:
Received 30 October 2012
Received in revised form 1 May 2013
Accepted 9 May 2013
Available online 1 July 2013

Keywords:
Ethanol
Acetic acid
Platinum
Tin
Alloy
Hydrogenation

ABSTRACT

Supported bimetallic Pt–Sn catalysts with different carriers were prepared through a one-step reduction method for the gas phase hydrogenation of acetic acid to ethanol. The structure of the catalysts was characterized by X-ray diffraction, transmission electron microscopy and energy-dispersive X-ray spectroscopy. Among these catalysts, the carbon nanotube-supported bimetallic Pt–Sn catalyst (Pt–Sn/CNT) showed the best performance, exhibiting over 97% conversion and 92% selectivity to ethanol under relatively mild conditions. The addition of Sn to Pt catalyst inhibited the C—C bond cleavage activity and enhanced the selectivity of the catalyst to ethanol, due to the formation and well-dispersion of PtSn alloy on the CNT surfaces. The catalytic performance depended on the ratio of Sn and Pt and the particle size of PtSn alloy. The one-step reduction method was conductive to preparing catalyst with smaller PtSn alloy particles and higher performance, which was shown that the optimized Pt–Sn/CNT with average PtSn alloy particle size at 3.0 nm can retain its high catalytic performance for over 300 h on stream.

1. Introduction

Ethanol (EtOH) is an important fundamental chemical. It can also be used as a gasoline additive to increase octane number and reduce CO_x, NO_x, and SO_x emissions [1]. Conventionally, EtOH is produced from feedstocks, such as oil and edible grains [2–5]. However, with the soaring prices of those resources, the development of new processes for EtOH production is highly demanded. The conversion of renewable cellulosic materials to EtOH is promising; however, considerable R&D efforts must be made before commercial-scale production can be achieved [6]. The direct approach of syngas-to-EtOH has drawn a great deal of attention because of the availability of syngas from coal, biomass, and natural gas (including conventional natural gas and unconventional gas such as shale gas, coal bed gas and tight gas) [7–11]. Nonetheless, the process has unsolved drawbacks, including low conversion and poor selectivity of EtOH because of the slow initial formation kinetics of the C–C bond and the fast chain growth of the C_2 intermediates [7,12]. EtOH can be obtained through the hydrogenation of dimethyl oxalate or the combined carbonylation of dimethyl ether and hydrogenation of methyl acetate [13,14]; however, disadvantages such as lower selectivity or overall atomic efficiency exist.

On the other hand, the technology of methanol carbonylation to acetic acid (AcOH) has been well developed [15,16] and the global AcOH had an overcapacity of more than 40% in 2010 [17]. AcOH can also be synthesized from syngas with supported Rh catalysts [18,19]. Thus, one of the alternative processes for the synthesis of EtOH *via* syngas is through the selective hydrogenation of AcOH ($CH_3COOH + 2\ H_2 \rightarrow CH_3CH_2OH + H_2O$, $\Delta H_{298} = -77$ kJ/mol) (Scheme 1) [20–22]. This process is an integrated technology consisting of syngas to methanol, coupling with CO to form AcOH, and subsequent hydrogenation to produce EtOH. The overall atomic efficiency from syngas to EtOH using the process is as high as 71.9%, similar to that obtained *via* the direct approach of syngas-to-EtOH. A number of noble metal-based catalysts are capable of catalyzing the conversion of different acids to corresponding alcohols [23,24]. Several groups have also reported that AcOH hydrogenation to EtOH can be readily accomplished over Pt-, Ru-, Pd-, and Re-based catalysts based on the density functional theory calculations or experiments [25–29]. A number of patents indicated that bimetallic catalysts containing Pt are effective for the hydrogenation of acetic acid to EtOH [30,31]. However, most of these catalysts suffer from lower EtOH productivity or harsh reaction conditions. Therefore, more detailed studies on the correlation between catalyst structure and performance are still necessary.

Bimetallic catalysts often exhibit novel properties because of the bifunctional mechanism or electronic effects [32–34]. The addition of a second metal also restrains the aggregation of monometals [35,36]. Meanwhile, the supermechanical, thermal, and electrical

* Corresponding author. Tel.: +86 592 2181659; fax: +86 592 2183047.
E-mail addresses: zxxie@xmu.edu.cn (Z. Xie), yzyuan@xmu.edu.cn (Y. Yuan).

0920-5861/$ – see front matter © 2013 Elsevier B.V. All rights reserved.
http://dx.doi.org/10.1016/j.cattod.2013.05.002

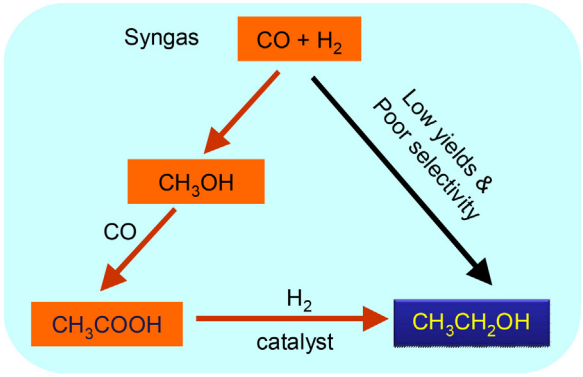

Scheme 1. Comparison of direct and indirect approaches for EtOH synthesis from syngas.

properties of carbon nanotubes (CNTs) and their one-dimensional characteristic have led to increased interests in the study of CNT-based devices and composites, including heterogeneous catalyst supports and promoters [37–42].

It is well-known that Pt–Sn bimetallic catalysts can be used in many reactions, such as hydrogenation [43–45], dehydrogenation [46,47], and oxidation reactions [48,49]. In most cases, Sn is added to Pt catalysts to enhance the selectivity. For example, Sn species can interact with the oxygen atom in the carbonyl group of an unsaturated aldehyde and hinder the activity of Pt toward the hydrogenation of the C=C bond. As a result, Pt–Sn catalysts show enhanced selectivity to unsaturated alcohol [50]. The current study reports that the Pt–Sn bimetallic catalyst supported on CNTs can exhibit remarkable performance for the hydrogenation of AcOH to EtOH under mild conditions. The catalytic behavior and the structural feature of the catalyst are addressed with a combination of kinetic and characteristic studies.

2. Experimental

2.1. Catalyst preparation

Supported bimetallic Pt–Sn catalysts were prepared *via* a one-step reduction method. CNTs (10–20 nm in diameter) with a purity of 95% were purchased from Shenzhen Nanotechnologies Port Co., Ltd. Hexachloroplatinic acid ($H_2PtCl_6{\cdot}6H_2O$), tin(II) chloride dihydrate ($SnCl_2{\cdot}5H_2O$), ethylene glycol (EG), sodium borohydride ($NaBH_4$), and sodium dodecyl sulfate (SDS) were purchased from Sinopharm Chemical Reagent Co., Ltd. First, the pristine CNTs were purified and functionalized in concentrated HNO_3 (68 wt%) at 353 K for 16 h under refluxing conditions to remove amorphous carbon and the remaining catalyst residues. The treated CNTs were filtered, extensively washed with deionized water until the pH of the rinsing water became neutral, and then dried at 373 K overnight. During the treatment, abundant surface functional groups, such as —COOH,)C=O, —OH and so on, were created on the surfaces of CNTs, which facilitated the uniform deposition of metal precursors. In a typical synthesis, initially purified CNTs were dispersed in EG by ultrasonic treatment (160 W and 40 Hz) for 30 min. The H_2PtCl_6 (3.7 mg mL^{-1}) and $SnCl_2$ (4.0 mg mL^{-1}) solutions were uniformly mixed. Subsequently, the mixture and a SDS solution (0.6 mg mL^{-1}) were mixed with the CNTs under agitation for 1 h. Here, EG acted as a dispersing agent to efficiently separate CNTs, whereas SDS acted as a stabilizer to drive the high dispersion of small nanoparticles on the surface of CNTs. Afterward, excess $NaBH_4$ solution was added dropwise to the mixture. After stirring for 5 h, the mixture was filtered, rinsed with deionized water, and then dried. Subsequently, the solid sample was calcined at 623 K for 4 h in air. The obtained solid were labeled as *x*%Pt–*y*%Sn/CNT, where *x* and *y* represent the weight percentage. The Pt–Sn catalysts with other supports, such as ZrO_2, TiO_2, SiO_2, and SiC, were prepared using the same procedure.

For comparison, the 1%Pt–2%Sn/CNT-IM catalyst was prepared *via* the co-impregnation method. Up to 1.0 g CNTs were dissolved in the mixture of the aqueous solution of H_2PtCl_6 (3.7 mg mL^{-1}) and $SnCl_2$ (4.0 mg mL^{-1}) under stirring. After completely dried at 333 K, the solid was calcined at 623 K for 4 h in air, and then reduced in a 5%H_2–95%N_2 at 623 K for 4 h.

2.2. Catalyst characterization

N_2 sorption isotherm was measured at 77 K using a Micromeritics TriStar II 3020 porosimetry analyzer. The samples were degassed at 573 K for 3 h prior to the measurements. The specific surface area was calculated according to the Brunauer–Emmett–Teller (BET) method.

Powder X-ray diffraction (XRD) patterns were taken using a Philips PANAlytical X'pert Pro diffractometer equipped with a graphite monochrometer and Cu K_α radiation (40 kV and 30 mA). The diffraction lines were identified by matching them with reference patterns in the JCPDS database.

Transmission electron microscopy (TEM) images and energy-dispersive X-ray spectroscopy (EDS) were taken using a Tecnai F30 electron microscope operated at an acceleration voltage of 300 kV. The powder was dispersed in ethanol by ultrasonication for 10 min, and then drops of suspensions were deposited on a copper grid coated with carbon. The statistical mean diameter of the nanoparticles was measured by counting at least 300 particles for each catalyst.

X-ray photoelectron spectroscopy (XPS) was performed using a Quantum 2000 Scanning ESCA Microprobe instrument (Physical Electronics). The samples were reduced and sealed immediately under Ar and then they were transferred to a UHV chamber to avoid contacting with air as much as possible. The raw data were corrected for substrate charging with the BE of C 1s peak (284.6 eV). Peak deconvolution and fitting were performed using the peak-fitting software with the spin–orbit splitting and the relative intensities of the spin–orbit components fixed. No trace of boron or sodium was detected on the reduced catalyst samples using XPS.

The metal dispersions and active surface area of the catalyst sample were determined by O_2–H_2 titration on a Mircometrics ASAP 2020 instrument. The reduced sample was evacuated at 313 K for 30 min, followed titrated with O_2 to form Pt_s–O and Sn_s–O species on the surface. After that, the H_2 adsorption was taken at 313 K to measure the amount of Pt_s–O species, according to literature [51], Sn_s–O species could not titrated with H_2. So the dispersion of metal Pt was calculated by assuming $H/Pt_s = 3$ stoichiometry due to the following reactions:

$$Pt_s + 1/2O_2 \rightarrow Pt_s\text{–}O \quad (1)$$

$$Pt_s\text{–}O + 3/2H_2 \rightarrow Pt_s\text{–}H + H_2O \quad (2)$$

2.3. Catalytic testing

The hydrogenation evaluation of the catalysts was carried out in a stainless steel tubular fixed bed reactor equipped with a computer-controlled auto-sampling system. About 200 mg catalyst was placed in the center of the reactor, and both sides of the catalyst bed were packed with quartz powders. Pure H_2 was fed into the reactor and the system pressure was held at 2.0 MPa. AcOH was pumped into the reactor with varying weight liquid hourly space velocities ($WLHSV_{(AcOH)}$) using a Series III digital HPLC pump (Scientific Systems, Inc.). The outlet stream line from the

reactor was heated at about 473 K to avoid condensation of reaction products. After depressured to ambient pressure, the outlet stream was auto-sampled to a gas chromatograph (GC) equipped with a flame ionization detector and KB-Wax capillary column (30 m × 0.32 mm × 0.33 μm) to quantify EtOH, acetaldehyde (Ace-Al), ethyl acetate (EtOAc), acetone, CH_4, and AcOH. The outlet stream was then cooled to below 278 K. The uncondensed gas was auto-sampled to another GC equipped with a thermal conductivity detector and dual columns of Gaskuropack 54 (3 m) and active carbon (3 m) to quantify CH_4, CO_2, CO, C_2H_6. AcOH conversion and product selectivities were calculated using the calibrated area normalization method.

The initial turn over frequency (TOF) of the reaction was measured under the conditions where the AcOH conversion was lower than 20%. The TOF value was based on the Pt dispersion, indicating the moles of AcOH converted per hour by per mole of metal at the catalyst surface (mol-AcOH mol-Pt_{surf}^{-1} h^{-1}, for short h^{-1}).

3. Results and discussion

3.1. Effect of support

Effect of support for the catalytic activity of AcOH hydrogenation to EtOH was investigated on several supported Pt–Sn bimetallic catalysts with different carriers. Table 1 shows that 1%Pt–5%Sn/CNT yielded an AcOH conversion of 49% and 83% selectivity to EtOH. By contrast, the catalysts with other supports exhibited a much lower selectivity to EtOH, although some of them showed higher AcOH conversion under the conditions of 623 K, 2.0 MPa, H_2/AcOH molar ratio of 40, and 3.0 h^{-1} $WLHSV_{(AcOH)}$. The XRD patterns of 1%Pt–5%Sn on different supports indicated that the diffraction peaks of possible Pt, Sn or PtSn alloy were hardly observed in all samples (Fig. S1). Further, the TEM images in Fig. S2 showed that the metal particles were smaller than 5 nm in average size and well dispersed on supports for all samples. However, the property of support has a major function on the catalyst performance for the hydrogenation of AcOH. Pt–Sn catalyst on supports like TiO_2 and ZrO_2 gave acetone as the main product, probably due to the strong chemical interactions between acetic acid and these oxides [52]. Pt–Sn catalyst on a nearly neutral support SiO_2 showed active for the partial hydrogenation of acetic acid, giving higher selectivity to aldehyde. Previous works also reported that Pt–Sn/SiO_2 was used for the partial hydrogenation of furfural [53] and Pt–Fe/SiO_2 catalyzed the hydrogenation of acetic acid to acetaldehyde and ethyl acetate [26]. SiC and CNTs have high mechanical strength properties and are chemical inertness, making the Pt–Sn/SiC and Pt–Sn/CNT catalysts show an improved selectivity to EtOH. In addition, CNTs are useful to concentrate the reactants in an area close to the active metal [54]. The better thermal conductivity of CNTs may also be beneficial for the exothermic catalytic reduction of AcOH [42]. The effects endow the Pt–Sn/CNT with higher catalytic performance in terms of conversion and selectivity.

The results in Table 1 also indicated that there is no direct relationship between the performance and BJH specific surface area (S_{BET}) of the catalyst, but the AcOH conversion may be related to the Pt surface area. The results on this issue are presented hereinafter in connection to the TOF of the catalysts.

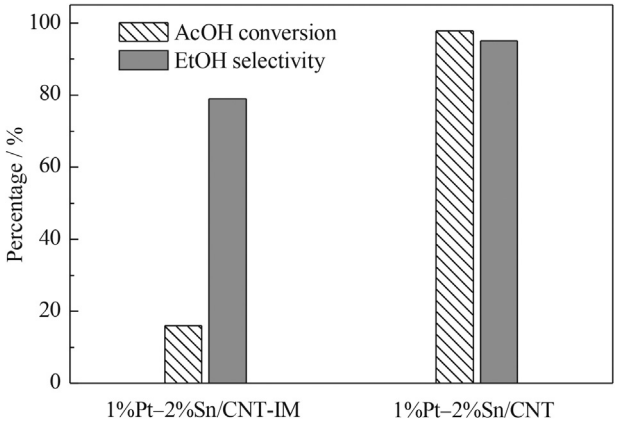

Fig. 1. Comparison of the catalytic performance of 1%Pt–2%Sn/CNT and 1%Pt–2%Sn/CNT-IM under the reaction conditions of 623 K, 2.0 MPa, $WLHSV_{(AcOH)}$ = 0.6 h^{-1}, and H_2/AcOH = 80.

3.2. Effect of catalyst preparation method

The catalytic performance of the 1%Pt–2%Sn/CNT catalyst was compared with that prepared *via* the conventional impregnation method (1%Pt–2%Sn/CNT-IM) under the following conditions: 623 K, 2.0 MPa, H_2/AcOH molar ratio of 80, and 0.6 h^{-1} $WLHSV_{(AcOH)}$. The results are shown in Fig. 1. It is easier to conclude that AcOH conversion and EtOH selectivity over 1%Pt–2%Sn/CNT are higher than those over 1%Pt–2%Sn/CNT-IM. We noticed that the activity of metal particles within the channels or dispersed on the outside surfaces of CNTs may have much different properties in catalysis [55]. We checked that the most of PtSn particles in 1%Pt–2%Sn/CNT were formed on the external surface of the nanotubes but some of them were positioned within the internal channels. Then we tried to prepare the catalysts with PtSn nanoparticles dispersed on the inside or outside surfaces of CNTs in different ratios. The experiments for the sample preparation were tough to reproduce. However, the catalytic performance was producible if the PtSn alloy nanoparticles were smaller and highly dispersed on the inside or outside surfaces of CNTs, always showing high performance for the hydrogenation of AcOH. Nevertheless, we could not exclude the confinement effect of the PtSn nanoparticles at present.

The structure of the Pt–Sn catalysts was then examined by XRD and TEM. The diffraction peaks marked as "#" correspond to the contribution of CNTs (Fig. 2). The diffraction peaks of possible PtSn alloy were observed in 1%Pt–2%Sn/CNT-IM sample, but were negligible in 1%Pt–2%Sn/CNT. The results suggest that the bimetallic nanoparticles in 1%Pt–2%Sn/CNT-IM were larger than those in 1%Pt–2%Sn/CNT. Further, the TEM images of the as-reduced catalysts in Fig. 3 show that the metal particles in 1%Pt–2%Sn/CNT-IM

Table 1
Hydrogenation of acetic acid over several supported 1%Pt–5%Sn catalysts[a].

Catalyst	S_{BET}, m^2 g^{-1}	S_{Pt}, m^2 g^{-1}	Conv., %	Selec., %				
				EtOH	Ace-Al	EtOAc	Acetone	$CH_x + CO_x$
1%Pt–5%Sn/ZrO_2	11	5.2	39.7	8.7	8.5	25.4	57.1	0.3
1%Pt–5%Sn/TiO_2	44	8.4	95.8	18.9	3.6	7.1	62.1	8.3
1%Pt–5%Sn/SiO_2	235	2.3	16.5	11.1	28.2	52.2	6.9	1.6
1%Pt–5%Sn/SiC	29	4.9	17.0	41.5	18.0	37.4	1.6	1.5
1%Pt–5%Sn/CNT	180	6.2	49.1	82.5	9.0	7.4	0.4	0.7

[a] Reaction conditions: 623 K, 2.0 MPa, $WLHSV_{(AcOH)}$ = 3 h^{-1}, H_2/AcOH = 40; $CH_x = CH_4 + C_2H_6$, $CO_x = CO + CO_2$.

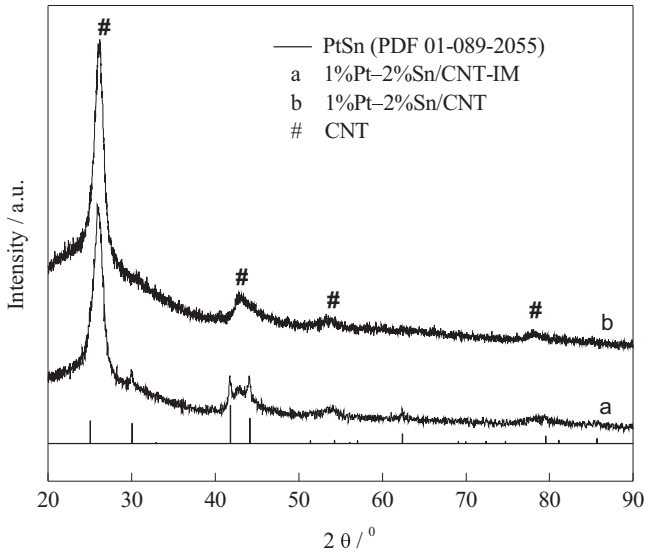

Fig. 2. XRD patterns of (a) 1%Pt–2%Sn/CNT-IM and (b) 1%Pt–2%Sn/CNT.

were aggregated, whereas those in 1%Pt–2%Sn/CNT were smaller and uniformly dispersed on the CNT surfaces. Fig. 4 shows the HR-TEM image and EDS of 1%Pt–2%Sn/CNT. The EDS measurements were taken for the selected Pt–Sn nanoparticles. Well-resolved lattice fringes were clearly observed, and two types of lattice fringes with interplanar spacings of 0.30 nm and 0.22 nm appeared, which are ascribed to the (1 0 1) and (1 1 0) planes, respectively. The angle between the planes was 47° (Fig. 4a). The results were approximate to the theoretical value of PtSn alloy nanocrystal (PDF 01-89-2055). The EDS in Fig. 4b revealed that the Pt–Sn alloy nanoparticle was consisted of Pt and Sn with an atomic ratio of approximately 1:1. The above results strongly suggest that the PtSn alloy was formed on the CNT surfaces. The 1%Pt–2%Sn/CNT with smaller size of PtSn alloy afforded higher performance of AcOH hydrogenation to EtOH.

3.3. Effect of Pt to Sn atomic ratio

A series of supported Pt–Sn bimetallic catalysts with fixed Pt loading at 1 wt% and varying Sn loadings at 0% to 5 wt% were prepared. The TEM images of the 1 wt% Pt monometallic and 1%Pt–*x*%Sn bimetallic catalysts supported on CNTs and the corresponding metal particle size distributions are represented in Fig. S3. The metal particles for all samples were well dispersed on the CNTs. However, the sizes of the nanoparticles for bimetallic catalysts were smaller than monometallic Pt. The presence of an appropriate amount of Sn can improve the dispersion of Pt nanoparticles and prevent the Pt nanoparticles from aggregation.

Fig. 5 displays the AcOH conversion and EtOH selectivity as a function of Sn loading in 1%Pt–*x*%Sn/CNT. The addition of Sn into Pt/CNT significantly enhanced EtOH selectivity. With the increase of Sn content from 0 wt% to 5 wt%, AcOH conversion displayed a volcano trend, where the optimal Sn loading was around 1.2 wt%. Table 2 shows the $CO_x + CH_x$ selectivity of AcOH hydrogenation, indicating that the monometallic Pt catalyst must have a high activity of C—C bond cleavage to form equal and much higher amounts of CO and CH_4 compared with bimetallic Pt–Sn/CNT.

Scheme 2 illustrates the Pt–Sn/CNT with different Sn contents and their catalytic behaviors in AcOH hydrogenation. Monometallic Pt nanoparticle is active for C—C bond cleavage. The PtSn alloy phase is formed when Sn is added to the Pt catalyst. With the increase of Sn content, Pt was almost completely alloyed with Sn and the catalyst

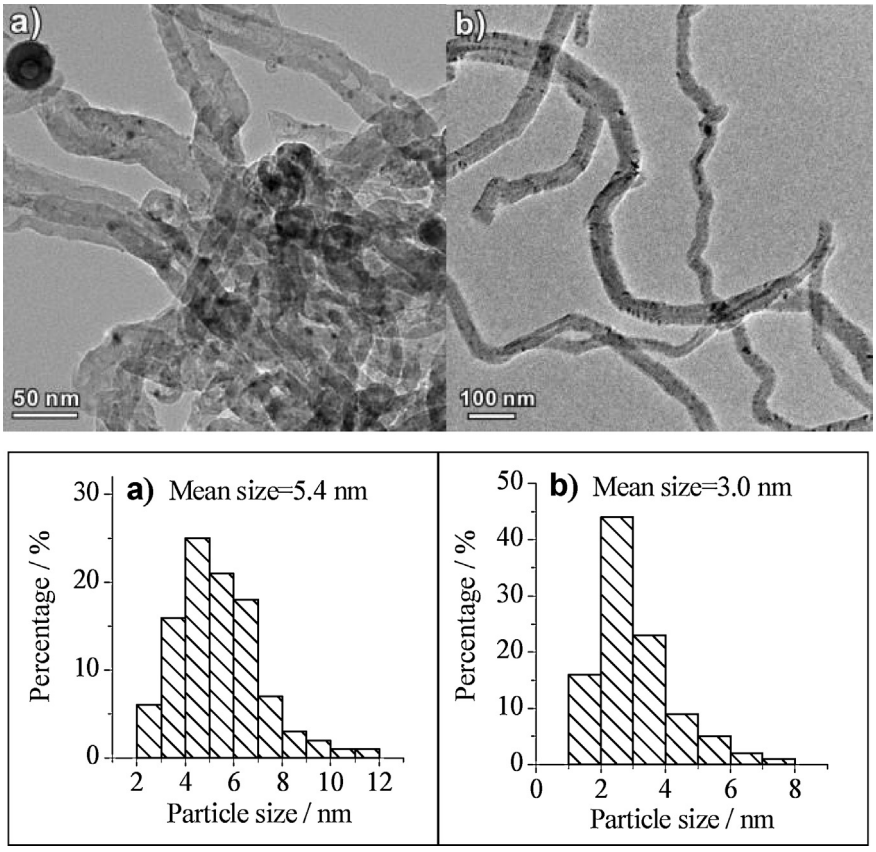

Fig. 3. TEM images and the metal nanoparticle distributions of (a) 1%Pt–2%Sn/CNT-IM and (b) 1%Pt–2%Sn/CNT.

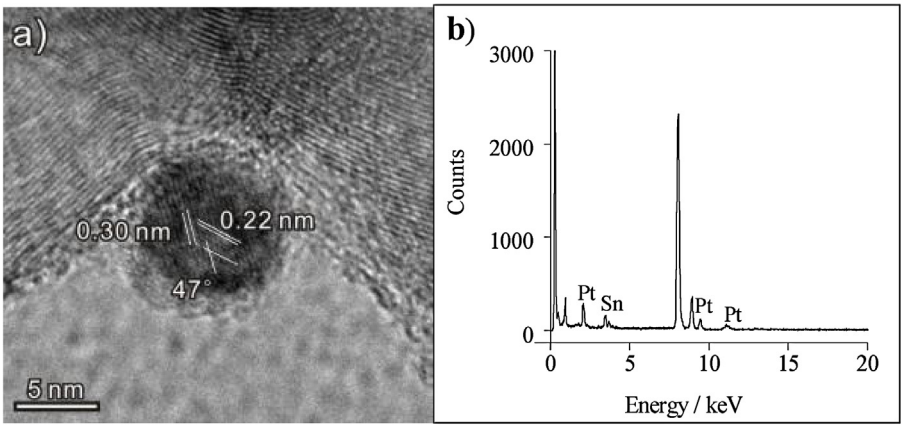

Fig. 4. HR-TEM image (a) and EDS (b) of 1%Pt–2%Sn/CNT.

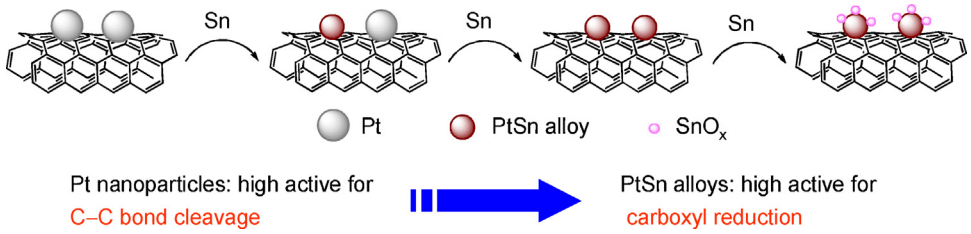

Scheme 2. Schematic for the preparation of Pt–Sn/CNT catalysts with different Sn contents and their catalytic behaviors in AcOH hydrogenation.

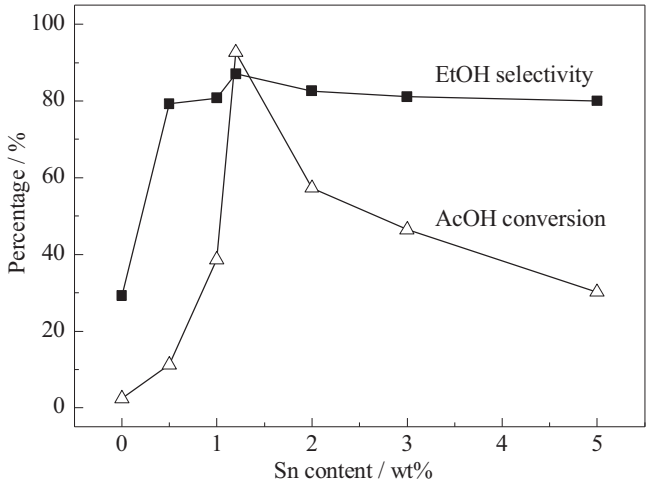

Fig. 5. Dependence of AcOH conversion and EtOH selectivity over 1%Pt–*x*%Sn/CNT as a function of Sn content under the reaction conditions of 623 K, 2.0 MPa, $WLHSV_{(AcOH)}$ = 3 h^{-1}, and H_2/AcOH = 40.

thus formed showed excellent activity for AcOH to EtOH by carboxyl reduction. However, excess Sn may present in oxidized form and cover the surface of PtSn alloy. In other words, when adequate Sn is added to the Pt catalyst, the resultant decreases the rate of C—C bond cleavage [29], but increases the reduction ability toward carboxyl group because of the formation of PtSn alloy. However, excess Sn loading can partially block the PtSn alloy active sites and suppress the catalytic activity.

In order to investigate the presence of oxidized Sn in as-reduced 1%Pt–3%Sn/CNT catalyst where excess Sn was loaded, the XPS measurement was carried out and the results are displayed in Fig. S4. The Sn $3d_{5/2}$ spectra showed two peaks. The first one with a binding energy of 485.5 eV can be attributed to zero-valent Sn, the second peak with a binding energy of 487.1 eV can be assigned to oxidized species Sn(II) and/or Sn(IV). It should be indicated that the distinction between Sn(II) and Sn(IV) species is not possible from the XPS measurements, since the two species have a slight difference in the binding energy [56].

There is a strong correlation between Pt dispersion (or Pt surface area) and hydrogenation performance of the catalyst. The TOF over the samples at 603 K increased markedly with the incorporation of small amount of Sn to Pt/CNT catalyst (Table 3). The highest TOF was obtained with the Pt–Sn/CNT catalyst containing 1.0 wt % Pt and 1.2 wt% Sn. Further increase of Sn loading caused a drop in TOF value. The results are in good accord with AcOH conversion as shown in Fig. 5.

Table 2
Comparison of selectivities to CO_x and CH_x over 1%Pt/CNT and 1%Pt–1.2%Sn/CNT.[a]

Catalyst	(CO_x + CH_x) Selectivity, %				Σ, %
	CO	CH_4	CO_2	C_2H_6	
1%Pt/CNT	33.1	33.2	0.7	0.8	68.7
1%Pt–1.2%Sn/CNT	1.3	1.3	0.3	0.4	3.3

[a] Reaction conditions are the same as those in Table 1.

3.4. *Effect of reaction parameter*

Fig. 6 shows the catalytic performance of optimized 1%Pt–1.2%Sn/CNT under different reaction parameters, including WLHSV, H_2/AcOH molar ratio, pressure, and temperature. Clearly, EtOH selectivity increased with the increase of AcOH WLHSV from 0.6 h^{-1} to 1.5 h^{-1}, and then decreased when AcOH WLHSV was higher than 3.6 h^{-1}. AcOH conversion gradually decreased with the increase in $WLHSV_{(AcOH)}$. AcOH conversion and EtOH selectivity decreased and increased with the increase of H_2/AcOH molar ratio from 20 to 100, respectively. Both AcOH conversion and EtOH selectivity slightly increased along with hydrogen pressure. However, AcOH conversion dramatically increased when the reaction temperature increased from 523 K to 623 K and reached a

Table 3
Results of O_2–H_2 titration and TOF over several supported Pt and Pt–Sn catalysts.

Sample	Metal dispersion, %		S_{Pt}, $m^2\ g^{-1}$	TOF at 603 K, h^{-1}
	By TEM[a]	By O_2–H_2 titration		
1%Pt/CNT	25.1	16.2	1.1	416.9
1%Pt–0.5%Sn/CNT	28.3	18.3	2.4	979.8
1%Pt–1.2%Sn/CNT	43.5	30.8	10.7	3242.1
1%Pt–2%Sn/CNT	37.7	20.5	8.6	2265.8

[a] All the Pt particles were regarded as the spheres. Thus, the Pt dispersion, D, was calculated as $D = (6\nu_m/\alpha_m d) \times 100\%$, according to literature [57], where, D is the Pt dispersion; ν_m is the volume of a Pt atom, $\alpha_m = (M/\rho N_o)$, M is the molecular weight of Pt, ρ is the density of Pt, N_o is Avogadro constant; α_m is the area of a Pt atom on the surface, $\alpha_m = 1/(1.25 \times 1019)$; and d is the Pt particle diameter determined by TEM. Therefore, $D = 1.13/d$.

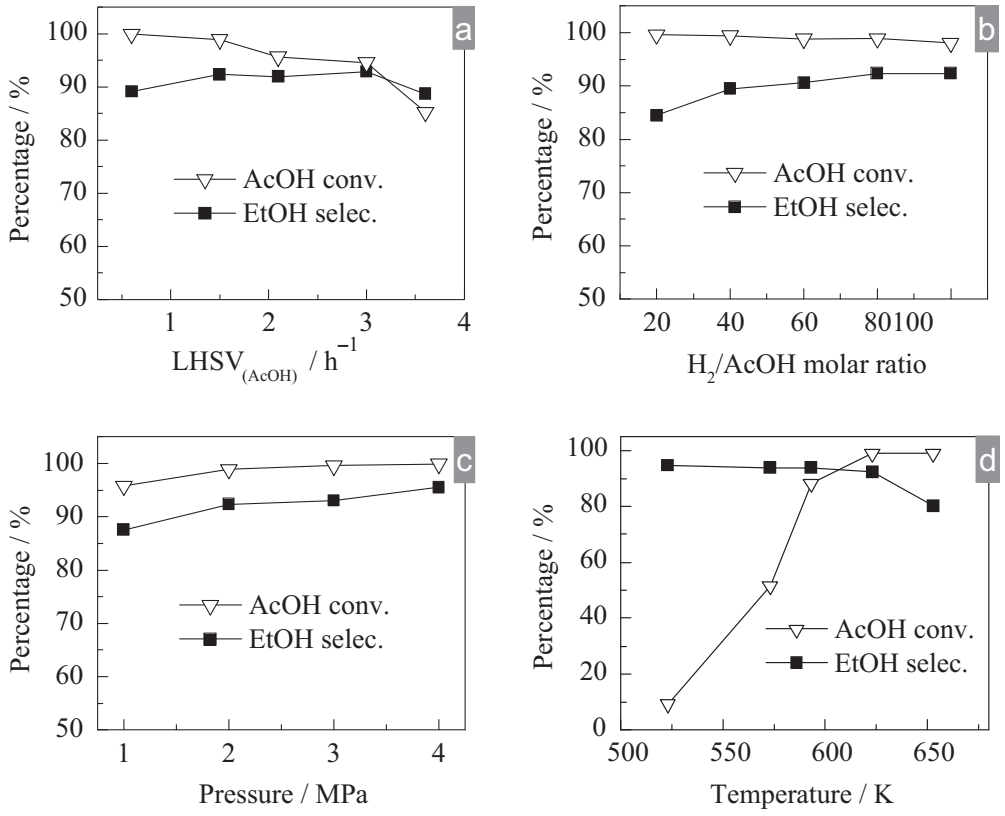

Fig. 6. Hydrogenation of AcOH over 1%Pt–1.2%Sn/CNT catalyst as a function of (a) AcOH WLHSV, (b) H_2/AcOH molar, (c) reaction pressure, (d) reaction temperature. Reaction conditions: 623 K, 2.0 MPa, H_2/AcOH = 80, $WLHSV_{(AcOH)} = 1.5\ h^{-1}$.

maximal plateau of 98.9% at temperatures higher than 623 K. EtOH selectivity obviously dropped at 653 K, probably due to the C—C bond cleavage at high temperature. Therefore, the vapor-phase hydrogenation of AcOH is sensitive to reaction parameters of reaction temperature, H_2/AcOH molar ratio, hydrogen pressure, and AcOH WLHSV.

3.5. Catalyst stability

The long-term stability and activity of the catalysts are important for AcOH hydrogenation to EtOH from both academic and industrial viewpoints. The long-term catalytic behavior of optimized 1%Pt–1.2%Sn/CNT is depicted in Fig. 7. The results demonstrated that 1%Pt–1.2%Sn/CNT retained its excellent activity for over 300 h at optimized reaction conditions of 623 K, 2.0 MPa, H_2/AcOH molar ratio of 80, and 1.5 h^{-1} $WLHSV_{(AcOH)}$. The XRD patterns of as-reduced 1%Pt–1.2%Sn/CNT and those after the reaction test for 300 h showed that only the diffraction peaks of the CNTs were observed on both catalysts, indicating that the PtSn alloy nanoparticles were not significantly aggregated after the catalytic

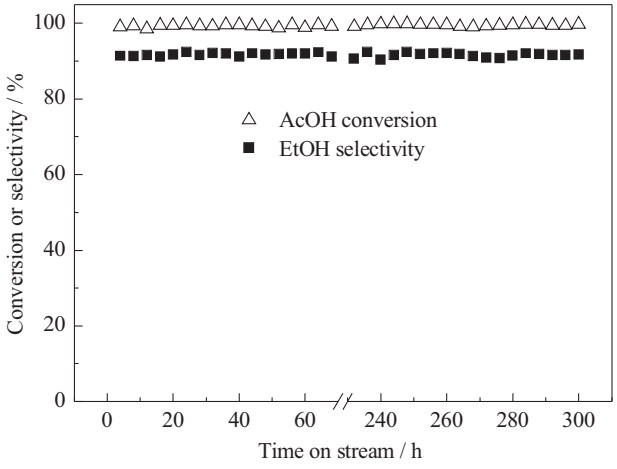

Fig. 7. Catalytic performance of 1%Pt–1.2%Sn/CNT as a function of reaction time under the reaction conditions of 623 K, 2.0 MPa, $WLHSV_{(AcOH)} = 1.5\ h^{-1}$, and H_2/AcOH = 80.

test for 300 h (Fig. S5). Consequently, the extraordinary activity and stability of the 1%Pt–1.2%Sn/CNT under the given operating conditions suggest that the catalyst is feasible and promising for EtOH production *via* the selective hydrogenation of AcOH.

4. Conclusions

PtSn alloy nanoparticles supported on CNTs were prepared *via* the one-step reduction method. The nanoparticles displayed better AcOH hydrogenation to EtOH than bimetallic Pt–Sn supported on other carriers. In addition, PtSn alloy nanoparticles were smaller and highly dispersed on the CNT surfaces compared with those prepared *via* the co-impregnation method. The addition of a suitable amount of Sn to Pt catalysts can promote the complete formation of PtSn alloy nanocrystals, which are highly active for the key step of the reduction of carboxyl group to attain excellent performance. Moreover, the optimized Pt–Sn/CNT sustained outstanding long-term stability and activity under relatively mild conditions.

Acknowledgements

We acknowledge the financial supports from the MOST of China (2011CBA00508), the NSFC (20923004 and 21173175), the Research Fund for the Doctoral Program of Higher Education (20110121130002), and the Program for Changjiang Scholars and Innovative Research Team in University (IRT1036).

Appendix A. Supplementary data

Supplementary data associated with this article can be found, in the online version, at http://dx.doi.org/10.1016/j.cattod.2013.05.002.

References

[1] J. Goldemberg, Science 315 (2007) 808–810.
[2] A.J. Ragauskas, Science 311 (2006) 484–489.
[3] C.J. Cleveland, C.A.S. Hall, R.A. Herendeen, Science 312 (2006) 1746–1748.
[4] T. Matsuzaki, K. Takeuchi, T. Hanaoka, H. Arawaka, Y. Sugi, Applied Catalysis A: General 105 (1993) 159–184.
[5] E.B. Pereira, G.A. Martin, Applied Catalysis A: General 103 (1993) 291–309.
[6] A.E. Farrell, R.J. Plevin, B.T. Turner, A.D. Jones, M. O'Hare, D.M. Kammen, Science 311 (2006) 506–580.
[7] X.L. Pan, Z.L. Fan, W. Chen, Y.J. Ding, H.Y. Luo, X.H. Bao, Nature Materials 6 (2007) 507–511.
[8] Y.M. Choi, P. Liu, Journal of the American Chemical Society 131 (2009) 13054–13061.
[9] J.J. Spivey, A. Egbebi, Chemical Society Reviews 36 (2007) 1514–1528.
[10] M. Haider, M. Gogate, R. Davis, Journal of Catalysis 261 (2009) 9–16.
[11] V. Subramani, S.K. Gangwal, Energy Fuels 22 (2008) 814–839.
[12] Y. Liu, K. Murata, M. Inaba, I. Takahara, K. Okabe, Catalysis Today 164 (2011) 308–314.
[13] J. Gong, H. Yue, Y. Zhao, S. Zhao, L. Zhao, J. Lv, S. Wang, X. Ma, Journal of the American Chemical Society 134 (2012) 13922–13925.
[14] G.H. Yang, X.G. San, N. Jiang, Y. Tanaka, X.G. Li, Q. Jin, K. Tao, F.Z. Meng, N. Tsubakia, Catalysis Today 164 (2011) 425–428.
[15] M.J. Howard, M.D. Jones, M.S. Roberts, S.A. Taylor, Catalysis Today 18 (1993) 325–354.
[16] G.J. Sunley, D.J. Watson, Catalysis Today 58 (2000) 293–307.
[17] Global Data, Acetic Acid: World Supply Outweighs Demand, 2011 (31 January).
[18] B.Q. Xu, W.M.H. Sachtler, Journal of Catalysis 180 (1998) 194–206.
[19] W.M. Chen, Y.J. Ding, D.H. Jiang, T. Wang, H.Y. Luo, Catalysis Communications 7 (2006) 559–562.
[20] B.W. Kiff, D.J. Schreck, US Patent 4421939, 1983.
[21] D. Verser, T. Eggeman, US Patent 6509180, 2003.
[22] R.C. Stites, J. Hohman, US Patent 0318573, 2009.
[23] M. Aly, E. Baumgarten, Applied Catalysis A: General 210 (2001) 1–12.
[24] T. Miyake, T. Makino, S. Taniguchi, H. Watanuki, T. Niki, S. Shimizu, Y. Kojima, M. Sano, Applied Catalysis A: General 364 (2009) 108–112.
[25] W. Rachmady, M.A. Vannice, Journal of Catalysis 192 (2000) 322–334.
[26] W. Rachmady, M.A. Vannice, Journal of Catalysis 209 (2002) 87–98.
[27] V. Pallassana, Journal of Catalysis 209 (2002) 289–305.
[28] H. Olcay, L. Xu, Y. Xu, G.W. Huber, ChemCatChem 2 (2010) 1420–1424.
[29] R. Alcala, J.W. Shabaker, G.W. Huber, M.A. Sanchez-Castillo, J.A. Dumesic, Journal of Physical Chemistry B 109 (2005) 2074–2085.
[30] V.J. Johnston, J.T. Chapman, L.Y. Chen, B.F. Kimmich, J.H. Zink, J.C. Waal, V. Zuzaniuk, US Patent 7608744, 2009.
[31] V.J. Johnston, L.Y. Chen, B.F. Kimmich, J.T. Chapman, J.H. Zink, H., Weiner, J.L. Potts, R. Jevtic, US Patent 0197485, 2010.
[32] M. Salciccioli, W. Yu, M.A. Barteau, J.G. Chen, D.G. Vlachos, Journal of the American Chemical Society 133 (2011) 7996–8004.
[33] Y. Tong, H.S. Kim, P.K. Babu, P. Waszczuk, A. Wieckowski, E. Oldfield, Journal of the American Chemical Society 124 (2002) 468–473.
[34] J. Greeley, M. Mavrikakis, Nature Materials 3 (2004) 810–815.
[35] Y. Wang, J.M. Zheng, K.N. Fan, W.L. Dai, Green Chemistry 13 (2011) 1644–1647.
[36] C.L. Bracey, P.R. Ellis, G.J. Hutchings, Chemical Society Reviews 38 (2009) 2231–2243.
[37] R.H. Baughman, A.A. Zakhidov, W.A. de Heer, Science 297 (2002) 787–792.
[38] B. Yoon, C.M. Wai, Journal of the American Chemical Society 127 (2005) 17174–17175.
[39] B.D. Li, J. Wang, Y.Z. Yuan, H. Ariga, S. Takakusagi, K. Asakura, ACS Catalysis 1 (2011) 1521–1528.
[40] M. Cargnello, M. Grzelczak, B. Rodríguez-González, Z. Syrgiannis, K. Bakhmutsky, V.L. Parola, L.M. Liz-Marzán, R.J. Gorte, M. Prato, P. Fornasiero, Journal of the American Chemical Society 134 (2012) 11760–11766.
[41] H.B. Zhang, X.L. Liang, X. Dong, H.Y. Li, G.D. Lin, Catalysis Surveys from Asia 13 (2009) 41–58.
[42] F. Deng, Q.S. Zheng, L.F. Wang, Applied Physics Letters 90 (2007) 021914 1–021914 3.
[43] G.C. Torres, S.D. Ledesma, E.L. Jablonski, S.R. de Miguel, O.A. Scelza, Catalysis Today 48 (1999) 65–72.
[44] S. Recchia, C. Dossi, N. Poli, A. Fusi, L. Sordelli, R. Psaro, Journal of Catalysis 184 (1999) 1–4.
[45] F. Coloma, A. Sepúlveda-Escribano, J. Fierro, F. Rodríguez-Reinoso, Applied Catalysis A: General 148 (1996) 63–80.
[46] O.A. Barias, A. Holmen, E.A. Blekkan, Journal of Catalysis 158 (1996) 1–12.
[47] R.D. Cortright, J.M. Hill, J.A. Dumesic, Catalysis Today 55 (2000) 213–223.
[48] A.E. Aksoylu, M.M.A. Freitas, J.L. Figueiredo, Catalysis Today 62 (2000) 337–346.
[49] B.S. Caglayan, I.I. Soykal, A.E. Aksoylu, Applied Catalysis B: Environmental 106 (2011) 540–549.
[50] J. Margitfalvi, I. Borbáth, M. Hegedűs, A. Tompos, Applied Catalysis A: General 229 (2002) 35–49.
[51] G. Corro, G. Aguilar, R. Montiel, S. Bernes, Reaction Kinetics and Catalysis Letters 73 (2001) 317–323.
[52] R. Pestman, R. Koster, A. Van Duijne, J. Pieterse, V. Ponec, Journal of Catalysis 168 (1997) 265–272.
[53] A.B. Merlo, V. Vetere, J.F. Ruggera, M.L. Casella, Catalysis Communications 10 (2009) 1665–1669.
[54] E. Castillejos, M. Jahjah, I. Favier, A. Orejón, C. Pradel, E. Teuma, A.M. Masdeu-Bultó, P. Serp, M. Gómez, ChemCatChem 4 (2012) 118–122.
[55] X. Pan, X. Bao, Accounts of Chemical Research 44 (2011) 553–562.
[56] C. Lau, G. Wertheim, Journal of Vacuum Science & Technology 15 (1978) 622–624.
[57] N. Mahata1, V. Vishwanathan, Journal of Catalysis 196 (2000) 262–270.